Check for updates

Starch bio-nanocomposites based on phosphorylated and sulphated cellulose nanocrystals extracted from pepper plant residue: effect of surface functionality on property improvements

Adil Bahloul · Fatima-Zahra Semlali · Mina Oumam · Hassan Hannache · Zineb Kassab · Mounir El Achaby

Abstract This work identifies Pepper (Capsicum annuum L) stems residue as a new potential source for producing high-quality cellulose nanocrystals (CNCs), making a significant contribution to the field of natural waste material utilization and sustainability. It also compares the properties of CNCs produced using two different acids, phosphoric acid and sulfuric acid (CNCPs and CNCSs), providing new insights into their properties and polymer reinforcing ability. Hence, the as-isolated CNCPs (D = 43 ± 15.11 nm, CrI = 84.78%) and CNCSs (D = 31 ± 8.80 nm, CrI = 85.41%) were separately dispersed in starch at different weight loadings, and their reinforcing effects on the chemical, morphological, thermal, transparency and mechanical properties of the resulting starch-based biocomposite films were discussed.

Globally, the incorporation of CNCs into starch biopolymer improved all these properties due to their rather similar polysaccharide structure and thus good interfacial interaction. However, the capacity of phosphoric acid to produce char made CNCPs effective flame retardants, thus providing bionanocomposite films with better thermal stability than CNCSs ones. In counterpart, the negative charge provided by the residual sulfate group (SO_4^{2-}) in CNCSs, coupled with their high aspect ratio, high surface areas and crystallinity, significantly improves the dispersibility of CNCSs in the ST matrix compared to the phosphoric acid-derived CNCs. Hence, adding up to 5 wt% CNCSs improved the film's transparency by 25%, stiffness by 196%, and ductility by 169%, compared to 11%, 164% and 114%, respectively, for CNCPs. Here, this work offers valuable insights into the utilization of pepper stems residue and the type of acid for CNCs production with outstanding characteristics.

A. Bahloul · M. Oumam · H. Hannache
Laboratoire d'Ingénierie Et Matériaux, Faculté Des Sciences Ben M'sik, Université Hassan II de Casablanca, B.P.7955, Casablanca, Morocco

F.-Z. Semlali (✉) · H. Hannache · Z. Kassab (✉) · M. El Achaby (✉)
Materials Science, Energy and Nanoengineering Department (MSN), Mohammed VI Polytechnic University (UM6P), Lot 660–Hay Moulay Rachid, 43150 Benguerir, Morocco
e-mail: fatimazahra.semlali@um6p.ma

Z. Kassab
e-mail: zineb.kassab@um6p.ma

M. El Achaby
e-mail: mounir.elachaby@um6p.ma

Introduction

Biomaterials are attracting more and more attention as environmentally friendly and sustainable materials

(Ouarhim et al. 2019; Oumayma et al. 2021; Semlali Aouragh Hassani et al. 2022b). Cellulose is considered to be one of the most important natural resources widely used in the production of paper and clothing, and is also starting to be used as a reinforcing material for bioenergy and composite materials (Espinosa et al. 2013; Semlali Aouragh Hassani et al. 2021a). Since nanoscience emerged, the manufacture of nanocellulose has proven to be a primary concern for both scientists and industry, as seen by the increase of papers and patents in this field. The advancement of nanocellulose research is motivated by its promising properties, including low cost, renewable nature, low toxicity, low density, high specific surface area, excellent optical transparency, and high mechanical properties (Rajinipriya et al. 2018; Semlali Aouragh Hassani et al. 2019b). Nanocellulose can be extracted from a variety of sources, including wood, natural fibers (agricultural biomass), marine animals (Ascaris suum), algae and fungi, thus their compositions depend to a large extent on the source. Nowadays, there is considerable interest in the use of agriculture waste (cotton stalk, rice straw, pineapple leaf, hemp, flax, rice husk, soy pods, potato peel, garlic straw, grape skin etc.) as the main feedstock for nanocellulose (Rajinipriya et al. 2018; Semlali Aouragh Hassani et al. 2020a). There are, however, still several untapped valuable cellulose-rich residues generated by the agriculture industry that haven't yet been valorized to produce cellulose structures.

Peppers (Capsicum annuum L.) are an important vegetable crop commonly consumed worldwide (Abd El-Mageed et al. 2020). The latter, can be of different colors (red, green, orange, and yellow) depending on their ripening stages and capacity to synthesize chlorophylls or carotenoids (Anaya-Esparza et al. 2021). It is well known that the fruit of pepper is usually divided into an edible part (pericarp and placenta) and an inedible part (seeds, pericarp and stem). The edible part of pepper has been reported to be an excellent source of polyphenols, especially flavonoids such as quercetin and luteolin, while the inedible parts are waste products of pepper processing. They have not received much attention (Chen and Kang 2014; Simonovska et al. 2016). Therefore, information on the extraction of cellulose and its derivatives from different parts of pepper and their physicochemical properties is limited (Simonovska et al. 2016). It is believed that harvesting of pepper produces a large

amount of plant residues, i.e., fiber-rich cellulose fibers, which are a good source for the extraction of new cellulose structures such as cellulose microfibers (CMFs), cellulose nanofibers (CNFs) and cellulose nanocrystals (CNCs).

Cellulose nanocrystals (CNCs) are attracting increasing interest as a possible way to improve the properties of biomaterials for a variety of applications mainly packaging, polymer nanocomposites, electronics, construction, cosmetics and biomedical purposes (Semlali Aouragh Hassani et al. 2021b; El Bourakadi et al. 2022). CNCs can be extracted from native cellulose by controlled hydrolysis with mineral acids (Ablouh et al. 2022). This process affords rigid rod-like single crystal domains with some desirable properties such as high aspect ratio (10–100), large specific surface area (~ 250–500 m^2/g), low density (~ 1.6 g/cm^3), high crystallinity (up to 90%), high tensile strength (7.5 GPa) and very high elastic modulus (100–140 GPa) (Fortunati et al. 2015; Kassab et al. 2019a). These properties are usually highly dependent on the cellulosic source and the chemical treatments used to produce them (Fortunati et al. 2015; Semlali Aouragh Hassani et al. 2020b). CNCs can be obtained mainly by strong acid hydrolysis using sulfuric acid or weak acid hydrolysis using phosphoric acid (Septevani et al. 2022). The acid hydrolysis process is a very well-known procedure that dissolves the amorphous part of cellulose, while leaving the crystalline part intact (Fortunati et al. 2015). Mukherjee and Woods were the first to use sulfuric acid hydrolysis to produce CNCs in 1953. It was found that CNC surfaces become negatively charged during the hydrolysis process when sulfate groups are introduced via the esterification of surface hydroxyl groups. Hence, the electrostatic attraction between CNCs caused by even small amounts of sulfate groups on their surfaces results in a good dispersion and stability of the aqueous suspension (Tian et al. 2016). The main disadvantage is that the sulfate groups accelerate the degradation of cellulose, which reduces the thermal stability of the final product, especially at high temperatures (Espinosa et al. 2013). Conversely, the phosphoric acid hydrolysis produced phosphorylated CNCs with embedded phosphate groups on the surface, resulting in colloidal suspension with low dispersibility but high thermal stability (Bahloul et al. 2021).

The incorporation of such CNCs with adjustable intrinsic properties is expected to enable production

of polymeric nanocomposites with tailored thermal, mechanical, barrier, and crystallization behavior (Dhar et al. 2016). Among biodegradable polymers, starch is the most widely used because of its renewability, abundant availability, low cost, and capacity to disintegrate without leaving harmful residues (Punia Bangar et al. 2022). However, despite its great commercial potential, starch has some drawbacks in terms of thermal, mechanical and barrier properties (Tibolla et al. 2020). Unquestionably, the incorporation of CNCs in starch polymer is expected to greatly enhance its properties due to their good compatibility and similar structure (Liu et al. 2018). In fact, the creation of hydrogen bonds between these two elements is encouraged by the homogenous dispersion of CNCs in the starch matrix. However, the type of acid hydrolysis, the CNC variation in aspect ratio and content alter the surface area in contact with the starch and obstruct the rearrangement of the starch chains during film formation (Liu et al. 2018).

We are aware of no publications describing either the isolation of pure cellulose nanocrystals from pepper agricultural residue or their capacity to reinforce starch polymers. The goal of this research is to examine the pepper stem residue as an unconventional renewable source for producing CNCs. The focus is to isolate phosphorylated (CNCPs) and sulfated (CNCSs) cellulose nanocrystals from newly identified cellulose-rich source. The physical and chemical characteristics of the as-produced CNCPs and CNCSs were described, and their synergistic impacts on the chemical, morphological, thermal, transparent, and mechanical characteristics of the resulting starch-based biocomposite films were assessed and discussed.

Materials and methods

Materials

Raw pepper (Capsicum annuum L) stems residue (R-PSR) was obtained from a Moroccan farm located at Benslimane city and affiliated to Casablanca-Settat administrative region. The starch used in this study has an average particle size of 45 μm and a density of 1.49 g/cm3. It was obtained from underutilized potato crops that were bought at a neighborhood market in Benguerir. One kilogram of potatoes yielded

about 80 g of starch, or an 8% yield. The commercial starch used for the comparison was purchased from sigma-Aldrich. The chemical reagents used were phosphoric acid (H_3PO_4, 85%), sulfuric acid (H_2SO_4, 95–97%), sodium hydroxide (NaOH, > 97%), glacial acetic acid (CH_3COOH, > 99%) and sodium chlorite ($NaClO_2$, 80%), and they were purchased from Sigma Aldrich. While glycerol (85%) was supplied by VWR. All chemical products were used as received without modification.

Extraction of pure cellulose microfibers (CMFs)

The procedure developed in our earlier works was followed for the extraction of CMFs (Khalili et al. 2023; Salim et al. 2023). Accordingly, the as received R-PSR fibers were first crushed into a length of 2 cm, then ground in a 0.5 mm sieve screen using a precision grinder and oven-dried for 40 min at 100 °C. The obtained fibers were immersed three times in NaOH aqueous solution (4 wt%) for 2 h at 80 °C under constant mechanical agitation, to remove partially the hemicellulose, lignin, and waxes from the fiber's cell wall's exterior surface. After the alkaline treatment, the fibers were filtered and rinsed with distilled water to undergo a bleaching process. The solution used in this treatment consisted of equal parts of acetate buffer (27 g NaOH and 75 ml glacial acetic acid, diluted to 1 L of distilled water) and aqueous sodium chlorite (1.7 wt% $NaClO_2$ in water) under atmospheric pressure and constant mechanical agitation for 2 h at 80 °C. Thereafter, they were filtered and rinsed with distilled water until neutralized pH. This treatment was done three times, resulting in pure white colored cellulose microfibers (CMFs). The fibers to liquor ratio in these treatments was 1/20 (g/mL).

Extraction of phosphorylated and sulfated CNCs

The CNCs were successfully extracted from the as-extracted cellulose microfibers (CMFs) using two different types of acids for hydrolysis (phosphoric acid (H_3PO_4) and sulfuric acid (H_2SO_4)), as developed in our previous works (Kassab et al. 2020c; Bahloul et al. 2021). For acid phosphoric treatment, CMFs were stirred in H_3PO_4 solution (9 mol/L) for 2 h at 100 °C, while for acid sulfuric treatment, they were stirred in H_2SO_4 solution (64 wt%) at 50 °C for 30 min. To stop the reaction, the acidic suspensions

were diluted with ice cubes and rinsed with successive cycles of centrifugation (Ultracentrifuge 100NX, HITACHI CP-NX series) at 12,000 rpm and 15 °C for 15 min to remove the excess acid. To neutralize the pH of the acquired products, they were dialyzed against distilled water. The obtained aqueous CNCP and CNCS suspensions from the hydrolysis of phosphoric and sulfuric acids, respectively, were then subjected to a 5-min ultrasonography (BRANSON, Sonifier 250) and stored in the refrigerator until use.

Starch Extraction

Starch was extracted from underused potato crops and peels as described in the work of Semlali et al. (Semlali Aouragh Hassani et al. 2022a). The process begins with thoroughly washing potato crops to remove exterior contamination, followed by peeling and cutting them into small pieces to assist blending, resulting in a slurry that will be filtered through a 100 μm sieve and allowed to settle. To enhance the starch production, this process was repeated numerous times. The acquired white sediment was dried overnight in the oven before being stored for future use.

Bionanocomposite films processing

Potato starch films with added as-extracted CNCPs and CNCSs were prepared using a solvent casting technique, as described in our earlier studies (Kassab et al. 2019b; Khalili et al. 2023). Firstly, the prepared potato starch was dissolved in distilled water followed by the addition of glycerol as plasticizer, hydrochloric acid (0.1 M) and sodium hydroxide (0.1 M) to neutralize the mixture for 30 min at 95 °C under mechanical stirring. Simultaneously, suspensions containing 1, 3 and 5 wt% of CNCPs and CNCSs were ultrasonicated for 10 min and mechanically stirred with starch solution for 30 min. The obtained solutions were then poured into Petri dishes, air-dried at ambient temperature in a laboratory hood, and oven drying to evaporate water, resulting in the production of bionanocomposite films (referred as ST, ST-CNCPX, and ST-CNCSX, respectively, for neat starch film and starch composite film containing X = 1, 3 and 5 wt% of CNCPs and CNCSs).

Characterization techniques

The morphology of the extracted CMFs and the fracture surfaces of the elaborated bionanocoposites films was examined using a scanning electron microscope (SEM, HIROX SH 4000 M) operated at 15 kV. Before imaging, the samples were coated with a thin conductive carbon layer using an ion sputtering apparatus.

Using atomic force microscopy (AFM, Veeco Dimension ICON), the morphology and size of the extracted CNCs (CNCPs and CNCSs) were assessed. Freshly cleaved mica sheets were immersed in diluted CNC suspension and oven dried at 60 °C for 15 min. The analysis was carried out in tapping mode, with Veeco Data Analysis Software used for image processing and dimension calculations.

The functional groups of all the samples were identified using Fourier transform infrared spectroscopy (FTIR, Perkin-Elmer Spectrum 2000) with an ATR accessory. The FTIR spectra ranged from 4000 to 600 cm^{-1}.

On a diffractometer (D2 PHASER diffractometer, BRUKER), X-Ray diffractograms of the examined samples were obtained. Samples were scanned with *CuK* radiation (λ = 1.54056 Å) in the 2θ range of 5–50°, at 40 kV and 40 mA in voltage and current, respectively. The crystallinity index (*CrI*) was calculated according to Segal equation:

$$CrI = \frac{I_{200} - I_{am}}{I_{200}} \times 100$$

where I_{200} is the intensity of the 200-lattice plane at around 2θ = 22.8°, and I_{am} is the minimum in the intensity (as shown in Fig. 5) from the amorphous phase at approximately 2θ = 18.6° (French and Santiago Cintrón 2013).

Thermogravimetric analysis (TGA) was performed using a thermogravimetric analyzer apparatus (Discovery TGA, TA instruments) under a nitrogen atmosphere (25 mL/min) from 25 to 700 °C at a heating rate of 10 °C/min.

Ultraviolet–visible (UV–Vis) spectroscopy measurements were taken with a PerkinElmer LAMBDA 1050 spectrophotometer to study the optical transparency of the bionanocomposite films. The film samples were directly inserted in the

spectrophotometer test cell, with air serving as a reference. In the wavelength range of 200–800 nm, the films' optical transmittance was measured (Fig. 1).

Tensile tests were carried out at room temperature using a Universal Testing Machine Texture Analyzer (TA.XT plus) with a 5 kN load cell, a crosshead speed of 5 mm/min and a gauge length of 30 mm, according to ISO 527–5. As a result, the developed films were cut into $(10 \times 50 \text{ mm}^2)$ samples, and a representative value of 5 specimens was recorded.

Results and discussions

Cellulosic fibers characterization

Morphological characteristics

SEM and AFM observations were used to assess the impact of mechanical and chemical treatments on the morphology, dimensions, and surface characteristics of the resulting CMFs, CNCPs and CNCSs materials. Figure 2 shows that the as-isolated CMFs had a massy filamentous structure and individual microfibers with a smoother surface and regular diameter, demonstrating that all the cementing agents (hemicellulose, lignin and other extractives) had been eliminated (Bahloul et al. 2021). The average diameter of CMFs was determined at approximately 16.40 ± 4.58 μm, which is higher than that determined for CMFs extracted from Alfa fibers (10 μm) (El Achaby et al. 2018b), pineapple leaf (4 μm) (Fareez et al. 2018),

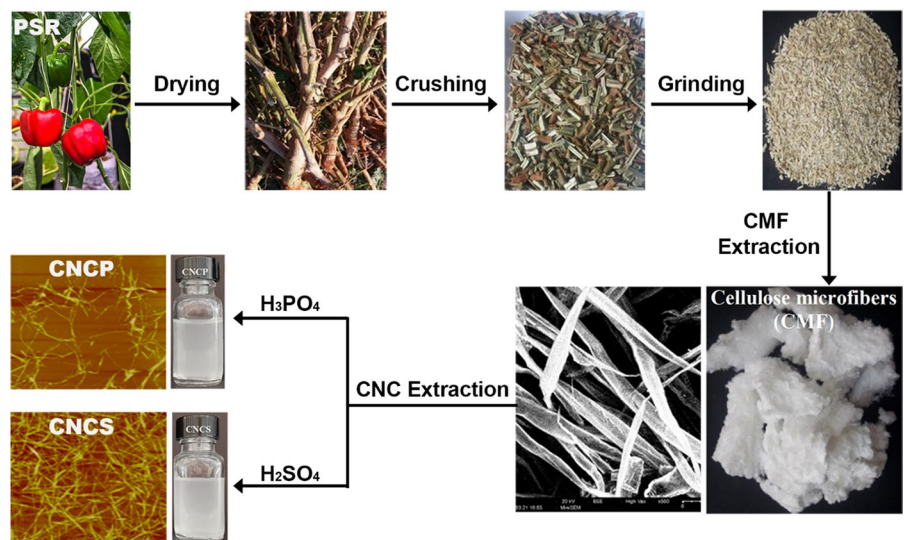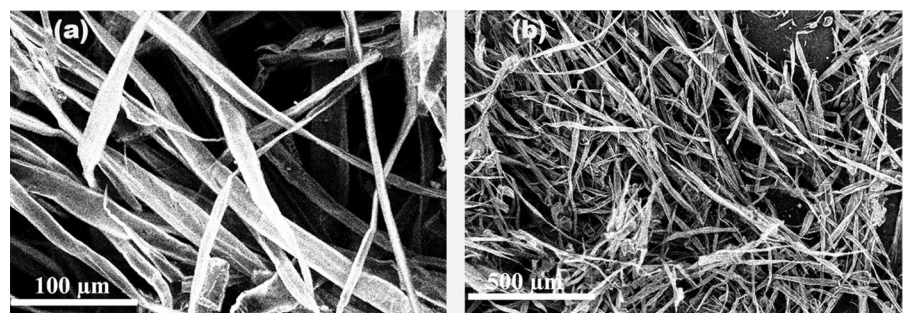**Fig. 1** Extraction stages of cellulose nanocrystals (CNCPs and CNCSs)

Fig. 2 SEM images of the extracted cellulose microfibers (CMFs)

Juncus stems (3.5 µm) (Kassab et al. 2020e), Hibiscus sabdariffa (10.04 µm) (Sonia and Priya Dasan 2013), and nearly equal to that of Hemp (16.96 µm) (Kassab et al. 2020a). Conversely, it presents an average diameter much smaller than sisal (287 µm) (Ludueña et al. 2013), cotton (131 µm) (Ludueña et al. 2013), and flax (51 µm) (Ludueña et al. 2013), and this by using the same chemical treatments. According to the literature, the purification methods used and the original cellulose sources have a significant impact on the morphology and diameter of bio-derived CMFs (Kassab et al. 2020b; Bahloul et al. 2021).

Unquestionably, it can be deduced that subjecting the newly identified R-PSR to conventional alkali and bleaching treatments results in an effective removal of all non-cellulosic components, and thus to the production of individual microsized cellulose fibers. More importantly, the obtained individual CMF may be suited for acid hydrolysis to dissolve the amorphous domains and convert the microscale into nanoscaled cellulose fibers. This was done by using two different acids for hydrolysis (phosphoric acid and sulfuric acid) to produce two types of nanoscaled cellulose (CNCPs and CNCSs) with different characteristics and different surface functionalities. Therefore, AFM observations were employed to assess their size and morphological characteristics in height and amplitude modes. From Fig. 3, it's evident that both CNCPs and CNCSs were successfully extracted from the recently discovered R-PSR, with well-defined needle-like shaped nanocrystal, uniform diameter, and an uneven length. The measured average diameters were 43 ± 15.11 nm and 31 ± 8.80 nm, respectively for CNCPs and CNCSs. The almost identical nanocrystal diameters in both cases suggest that the amorphous CMFs regions are equally cleaved laterally when hydrolyzed with phosphoric acid and sulfuric acid, respectively (Bahloul et al. 2021). However, CNCPs present a diameter relatively higher than CMFs hydrolyzed with phosphoric acid extracted from mulberry bark (25–30 nm) (Rajinipriya et al. 2018), tomato plant residue (6.2 ± 2.4 nm) (Kassab et al. 2020b), and eggplant plant (6.3 ± 2.3 nm), while being almost equal to Whatman filter paper (31 ± 14 nm) (Espinosa et al. 2013). In counterpart, CNCSs exhibit a diameter higher than sugarcane bagasse (5.0 ± 1.1 nm) (Kassab et al. 2019a), Alfa fibers (5 ± 3 nm) (El Achaby et al. 2018b), and Agave tequilana (11 ± 4 nm) (Espino et al. 2014). This funding demonstrates how the cellulose source and the hydrolysis processing parameters have a significant impact on the dimensions and features of CNCs (Rajinipriya et al. 2018).

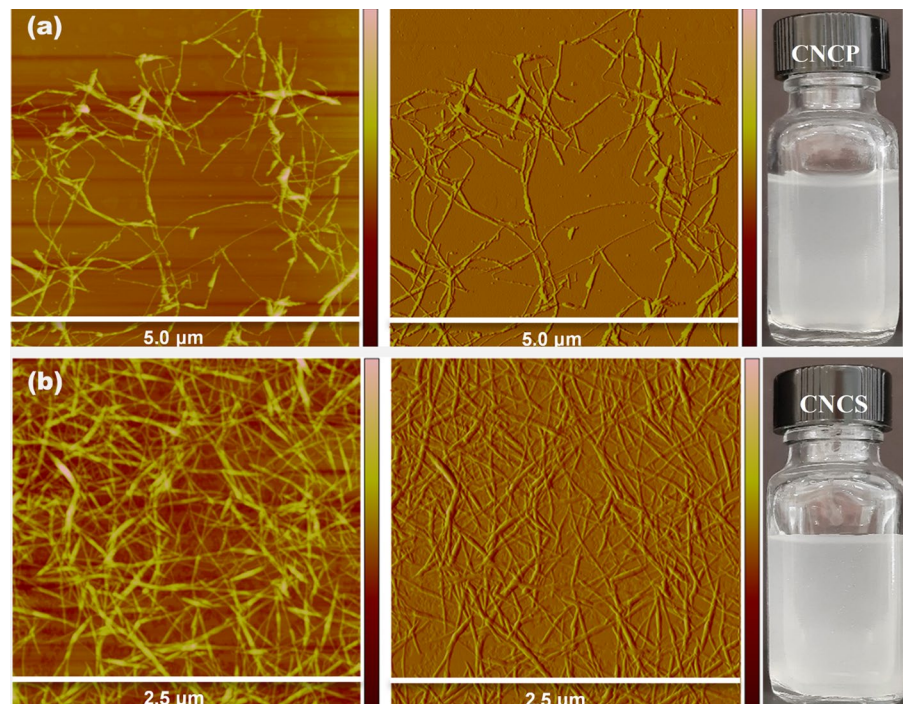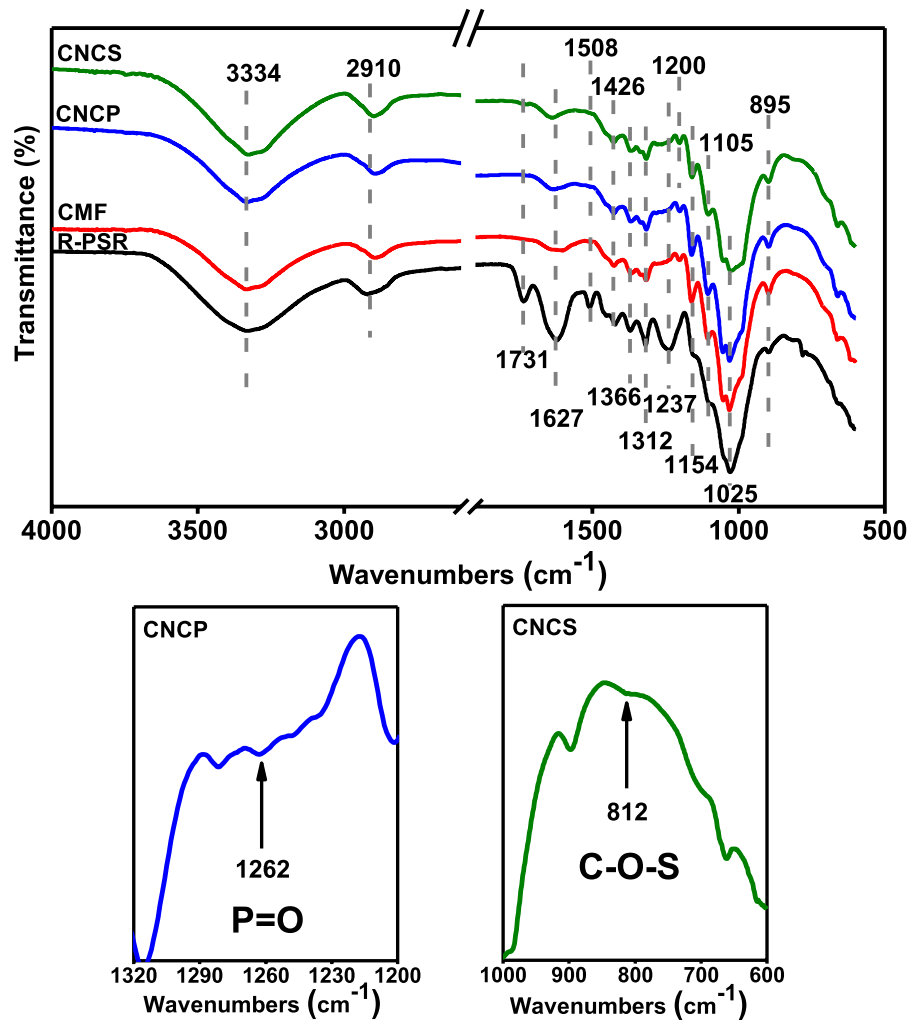**Fig. 3** AFM images of **a** CNCPs and **b** CNCSs

Fig. 4 FTIR spectra of cellulosic fibers

Chemical structure (FTIR)

The chemical composition and surface functionality of the isolated cellulose at various phases of treatment were analyzed using FTIR spectroscopic method and presented in Fig. 4. A cursory examination of the newly identified R-PSR reveals the presence of cellulose characteristic bands at 3334, 2910 and 1023 cm^{-1} assigned to stretching vibrations of hydrogen bond O–H, C–H symmetrical stretching, and glycosidic ether band C–O–C, respectively (Risite et al. 2022). The band at 1627 cm^{-1} corresponds to the O–H stretching and bending vibrations of the adsorbed water (Bahloul et al. 2021). Three peaks at 1731, 1508, and 1237 cm^{-1}, which are unique to the R-PSR spectrum represent C=O stretching vibration, C=C vibration of the aromatic skeleton, and C–O

stretching vibration of acetyl or aryl functional groups from hemicellulose and lignin fractions (Risite et al. 2022). However, the three peaks at 1426, 1366, and 1312 cm^{-1} were attributed to cellulose's CH2 symmetric bending, C-O symmetric stretching, and C-H bending (Bahloul et al. 2021). The band at 1154 cm^{-1} is attributed to the C–O stretching vibration and anomeric carbon of b-D-glucopyranosyl of cellulose (Kassab et al. 2019b), while the last peaks at 1105 and 895 cm^{-1} referred to the presence of β-glucosidic ether linkages (C–O–C) related to the vibration modes of anhydro-glucopyranose ring skeleton, and to the β-glycosidic linkages between the anhydroglucose rings in the cellulose (El Achaby et al. 2018a).

In the spectrum of CMFs, CNCPs and CNCSs, the disappearance of a few peaks associated with the presence of lignin and hemicelluloses (1731, 1508

and 1237 cm^{-1}) was clearly observed, confirming the complete removal of non-cellulosic components after bleaching and acid hydrolysis processes, whereas the characteristic bands of cellulose were maintained (Gan and Chow 2019; Salim et al. 2022a).

Since two distinct acids were employed to isolate CNCs, their FTIR spectral bands were compared to identify any notable modifications to CNCs' chemical structure due to the substitution of different chemical moieties. Thus, subjecting CMFs to acid phosphoric treatment led to the appearance of the peak characteristic of phosphate groups in CNCPs (P–O stretching vibration) located between 1275–1225 cm^{-1}. In contrast, the sulfuric acid hydrolysis led to the emergence of two tiny bands at 1200 cm^{-1} and 812 cm^{-1} linked to the sulfate groups (C–O–S vibration) injected into the surface of CNCs (El Achaby et al. 2018b; Xie et al. 2018). To conclude, the FTIR results confirmed the successful extraction of CMFs, CNCPs and CNCSs from the newly discovered Raw pepper (Capsicum annuum L) stems residue.

Crystalline structure

In order to understand the crystallites' physical characteristics and determine whether CNCs underwent polymorphic or chemical changes during acid hydrolysis treatments, XRD studies were performed (Dhar et al. 2016; Salim et al. 2022b). Hence, the crystalline structure and the crystallinity (determined using the Segal equation) described in the studied R-PSR and its cellulose derivative mainly CMFs, CNCPs and CNCSs were illustrated in Fig. 5. Realistically, all samples had the usual cellulose I structure, which can be distinguished by the principal crystalline peaks at roughly 15.2°, 16.8° and 22.7°, which correspond to the typical reflection planes (1 $\bar{1}$ 0), (110) and (200), respectively (French 2014). This indicates that the alkali, bleaching, and different acid hydrolysis treatments had no effect on the cellulose component's crystal structure (El Achaby et al. 2018b). As it's well known, cellulose is composed both extremely crystalline and disordered amorphous regions. It is thought that the increased crystallinity is caused by the removal of the disordered amorphous regions during extraction methods. Effectively, subjecting the starting material R-PSR to alkaline and bleaching treatments increased the crystallinity from 62.06% to 80.12%, thus confirming the successful partial
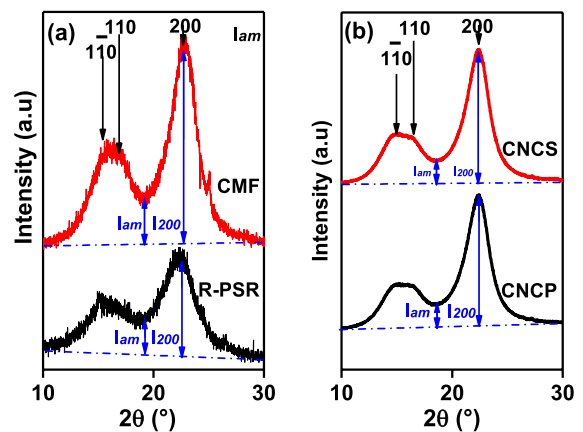

Fig. 5 XRD patterns of cellulosic fibers

removal of hemicellulose and lignin during chemical treatments (El Achaby et al. 2018a; Risite et al. 2022).

Chemical hydrolysis occurs when an acid attacks the amorphous regions of CMFs and initiates the hydrolytic breakage of glycosidic linkages, releasing individual crystallites and immediately increasing the crystallinity of cellulose (Risite et al. 2022). The crystallinity index gradually rose for CNCPs and CNCSs, from 80.12% for CMFs to 84.78% and 85.41%, respectively. These results confirmed that the amorphous portions were successively removed during acid hydrolysis (Bahloul et al. 2021; Salim et al. 2022c). This conclusion is consistent with FTIR analysis, which demonstrated that lignin and hemicellulose molecules were eliminated following the purification procedures used.

Additionally, it is presumed that the concentration of the used acids (phosphoric and sulfuric acids), the temperature of the hydrolysis, the contact time, the ratio of cellulosic biomass-to-acid used for hydrolysis, and the type of initial biomass chosen will all affect the crystallinity of the isolated CNCs (Dhar et al. 2016). Thus, because strong acid can more aggressively target the disorder or amorphous region than other mild acids, sulfuric acid hydrolysis is known as a promising approach to manufacture more crystalline CNCs (Septevani et al. 2022). As expected, CNCSs (85.41%) has a relatively high crystallinity than CNCPs (84.78%). Similar results were obtained in the study on eggplant plant (Solanum melongena L) agricultural residue using a similar

acid hydrolysis method. It was found that the crystallinity increased from 62% for raw fibers to 71%, 73%, and 80% for CMFs, phosphorylated CNCs, and sulfated CNCs, respectively (Bahloul et al. 2021). Therefore, it was confirmed using XRD measurements that using different hydrolyzing acids did not change the original cellulose crystal structure but had a substantial impact on the crystal characteristics of produced CNCs (Dhar et al. 2016). More crucially, CNCs' mechanical, thermal, and transparency characteristics are directly correlated with their crystallinity. To conclude, the developed highly crystalline CNCs could be regarded as effective nanoreinforcements for the development of high performant polymer bionanocomposite films (Bahloul et al. 2021).

Thermal stability

The degradation behavior and the thermal stability of the studied R-PSR and its cellulose derivatives are described in Fig. 6. All of the samples' TGA curves, clearly show a minor weight loss at temperatures between 60 and 110 °C corresponding to the water evaporation, which is related to the hydrophilic nature of the cellulosic materials (Gan and Chow 2019). The R-PSR was having another two weight loss peaks at $T_{max1} = 270.75$ °C and $T_{max2} = 328.05$ °C, respectively, after the water evaporation peak with a beginning degradation stage at $T_{onset} = 281.12$ °C. Raw natural fibers are typically renowned for having limited thermal stability, which makes it difficult to melt and blend them with most thermoplastic polymers (Semlali Aouragh Hassani et al. 2019a). Additionally, lignin, hemicellulose and cellulose were having different chemical structures, and these caused them

to decompose at different temperatures (Gan and Chow 2019). The temperature range between 250 and 300 °C shows the depolymerization of non-cellulosic components such as hemicelluloses and lignin. Further, it indicates the breakage of the glycosidic bonds. Whereas the temperature between 300 and 400 °C indicates the degradation of the α-celluloses (Sonia and Priya Dasan 2013).

Subjection of the R-PSR to the alkaline and bleaching treatment highly increase the thermal stability ($T_{onset} = 310.23$ °C), and the resulting CMFs showed one main degradation peak temperature at around 353.29 °C. This improved thermal stability is due to the removal of non-cellulose and amorphous components, which tend to lower the thermal stability, thus resulting in increased crystallinity and increased intermolecular hydrogen bonding domains (Risite et al. 2022). These results are therefore in agreement with the FTIR and XRD analyses. On the other hand, the residues left after heating at 600 °C were observed to be about 25.72 and 15.60 for R-PSR and CMFs, respectively. In fact, it was thought that the high levels of lignin and hemicellulose were responsible for the raw material's significant char residue (Sonia and Priya Dasan 2013).

However, the TGA curves of CNCPs and CNCSs are relatively similar (T_{max}(CNCPs) = 341.90 °C and T_{max}(CNCSs) = 341.50 °C), showing only a slight decrease in thermal stability compared to CMFs (353.29 °C). The acid hydrolysis procedures that bring phosphate and sulfate groups to the surface of the CNCs and reduce their thermal stability may be the basis of this behavior (Bahloul et al. 2021). Less energy was needed to break down the phosphate or sulfate anhydro-glucose unit, which resulted in lower

Fig. 6 thermal stability of cellulosic fibers: **a** TGA, **b** DTG
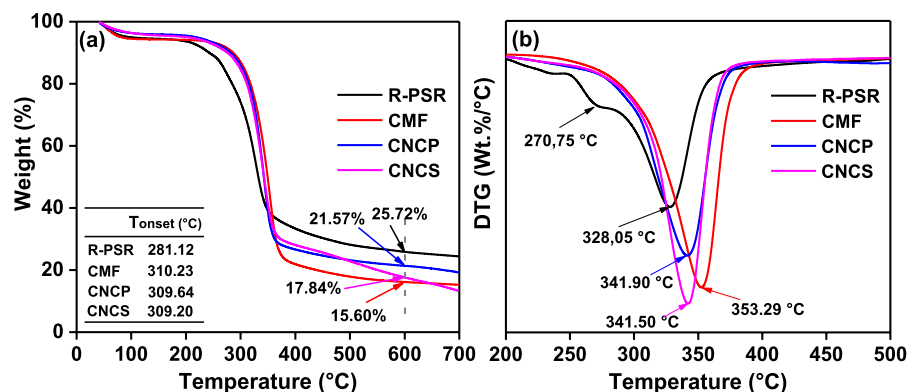
temperatures during the degradation process (Kassab et al. 2020a). Another factor contributing to the CNCs's lesser stability was acid hydrolysis, which eliminated the fiber's amorphous region and reduced the particle size, increasing the surface area and lowering the thermal degradation temperature. Due to the larger surface area of the CNCs, more chain free ends were exposed, which encourages degradation at lower temperatures (Gan and Chow 2019).

Besides that, both the CNCPs and CNCSs were having a higher percentage of remaining char residues than CMFs at 600 °C. The crystalline area of the CNCs, which would function as a charring agent at high temperatures, could explain this (Gan and Chow 2019; Kassab et al. 2020a). As the amount of carbon grows due to this extremely crystalline section of the CNCs, char residue is formed. The char residue of both CNCPs and CNCSs may be attributed to the dehydration mechanism carried out by phosphoric acid and sulphuric acid in addition to having more crystalline area (Gan and Chow 2019). Both phosphoric acid and sulfuric acid would hasten the degradation of cellulose by esterifying or catalyzing the removal of some of the -OH groups. The elimination of oxygen in the form of H_2O, which results in the dehydration process, would make the generation of char residue easier in the presence of the H+ ion. The creation of anhydrocellulose was encouraged by this process, and the anhydrocellulose's decomposition resulted in the generation of char (Gan and Chow 2019).

Apart from that, CNCPs have higher char residue (21.57%) compared to CNCSs (17.84%) at 600 °C. As is well known, phosphorus can act as a flame retardant in a variety of phases. In condense phase,

the phosphorus can make more char which leads to the yielding of intumescence. However, in gas phase, the phosphorus group is able to inhibit the flame. Therefore, it is plausible to conclude from this study that the char produced by the phosphate group had reduced the cellulose's exposure to the heat source, which can also explain the slight improvement of CNCPs thermal stability as compared to CNCSs (Gan and Chow 2019).

Chemical and crystalline structure of the extracted potato starch

The chemical and crystalline composition of the extracted (E-ST) and commercial (C-ST) potato starch were compared to demonstrate the starch's successful extraction (Fig. 7). FTIR spectroscopy is thought to be a useful method for structural changes in starch, such as starch chain conformation, helicity, crystallinity, and retrograde phase, at the molecular level (short order) (Semlali Aouragh Hassani et al. 2022a). This was done primarily to identify the extracted starch's key functional groups and to validate the starch's structural integrity. It is evident from comparing the two spectra that they displayed essentially identical shapes and peaks, suggesting that their chemical structures are similar (Fig. 7a). Thus, the main bands at 3290, 2915 and 1648 cm^{-1} are attributed to O–H group in starch skeleton, stretching vibration of –CH groups from glucose and H–O–H bending vibration of water molecules, respectively (Warren et al. 2016; Pozo et al. 2018). Furthermore, the three peaks located at 1429, 1145 and 1071 cm^{-1} are characteristic of CH_2 symmetric deformation, C–O–C asymmetric stretching, and C-O stretching,

Fig. 7 Comparison of the extracted and commercial potato starches for **a** chemical structure by FTIR, and **b** for crystal structure by XRD
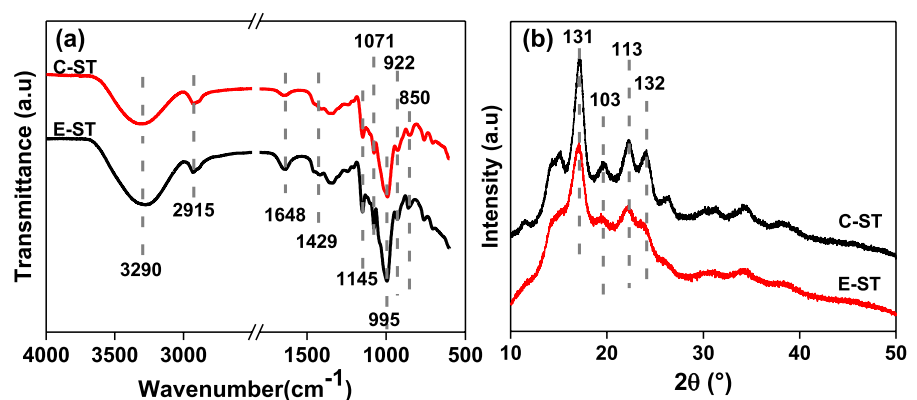
respectively (Warren et al. 2016; Pozo et al. 2018). However, the band 995 cm^{-1} is attributed to C-O stretch vibration in C–O–C groups (characteristic of polysaccharides), while the last two low peaks at 922 and 850 cm^{-1} were ascribed to C–O–C ring vibration in starch (de Azevedo et al. 2020; Semlali Aouragh Hassani et al. 2022a). All of these vibrations demonstrate that potato starch was successfully extracted, whereas the small changes in peak intensity are attributed to the variation in the moisture content and crystallinity of the extracted potato starch (Semlali Aouragh Hassani et al. 2022a). Hence, XRD analysis was used to explore the crystallinity and crystalline structure of the extracted and commercial starches, and the results are represented in Fig. 7b. As predicted, both starches exhibit the same characteristic peaks (17.22°, 19.62°, 22.28°, and 24.12°) that corresponds to the planes (131), (103), (113), and (132), demonstrating that potato starch has a B-type crystalline structure (Semlali Aouragh Hassani et al. 2022a). The small difference in the peak intensities can be attributed to

the extraction process conditions, which can harm the starch granules, as well as to variations in the amount of water and/or temperature used during the extraction process (Jagadeesan et al. 2020). This explanation is in perfect line with the FTIR results.

Chemical structure of bionanocomposite films

FTIR spectroscopy was used to understand the potential interactions between starch and different acid derived CNCs (CNCPs and CNCSs). The IR spectrum of neat starch film and nanocomposite films with various CNCPs and CNCSs content are shown in Fig. 8. As expected, the addition of CNCPs and CNCSs demonstrated an insignificant effect on the IR spectrum of ST films due to the absence of new peaks. All the films exhibited almost the same profile and bands, due to the chemical similarities between starch and cellulose being both polysaccharides (Balakrishnan et al. 2018). Therefore, it is impossible to identify a separate peak for each phase. However,
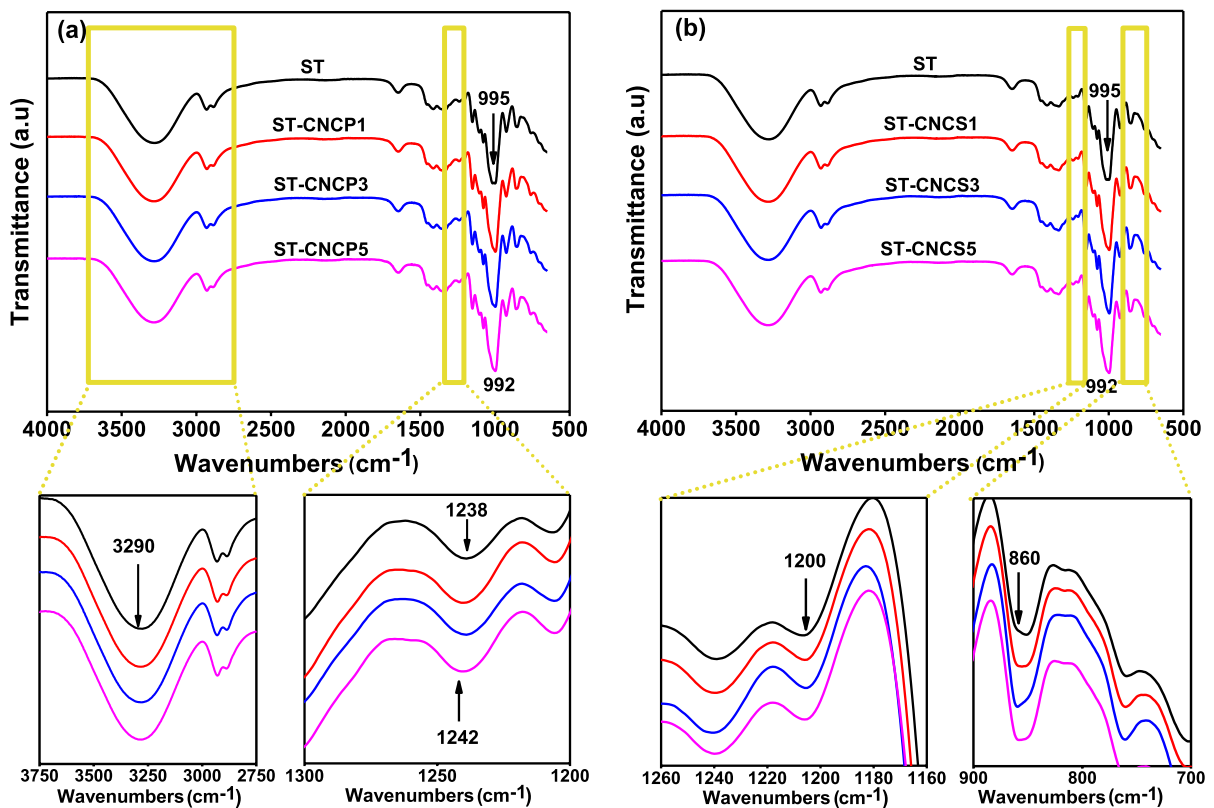

**Fig. 8** FTIR spectra of the elaborated bionanocomposites films

with the addition of CNCs, a gradual rise in the peak intensity related to the presence of the hydroxyl group of the polysaccharide starch and cellulose (3290 cm^{-1}) was seen, affirming the strong hydrogen bonding between cellulose and starch (Huang et al. 2019). Additionally, a deep analysis of the spectrum shows that the peaks used to indicate the presence of both phosphate and sulphate groups were really overlapped with starch molecules' characteristics peaks. Indeed, by increasing CNCP concentration up to 5 wt%, the peak related to the phosphate group became sharper and shifted from 1238 to 1242 cm^{-1}, while with the addition of CNCSs in starch polymer the bands associated with sulfate groups (1200 and 860 cm^{-1}) sharpened (Yadav and Chiu 2019; Septevani et al. 2022). Furthermore, by increasing both of CNCPs and CNCSs the peak wavenumber for C-O stretching vibrations altered from 995 to 992 cm^{-1}.

This change indicates that the incorporation of cellulose nanocrystals (CNCPs and CNCSs) into starch led to novel interactions, thus suggesting good CNCs/starch interfacial adhesion (Cao et al. 2008; Yadav and Chiu 2019).

Morphological properties of bionanocomposite films

Scanning Electron Microscopy (SEM) was used to observe the fracture surfaces of the elaborated samples and get some information about the effect of CNCs (CNCPs and CNCSs) on the starch morphology, as well as their interfacial adhesion. It is evident from Fig. 9 that the surface of the starch film was homogeneous, smooth, free of cracks, and uniform. The smoother surface was most likely caused by the continuous glycerol phase and gelatinization of the starch granules (Agustin et al. 2013). However, the

Fig. 9 SEM micrograph of bionanocomposite films at 3 wt% of CNCPs and CNCSs
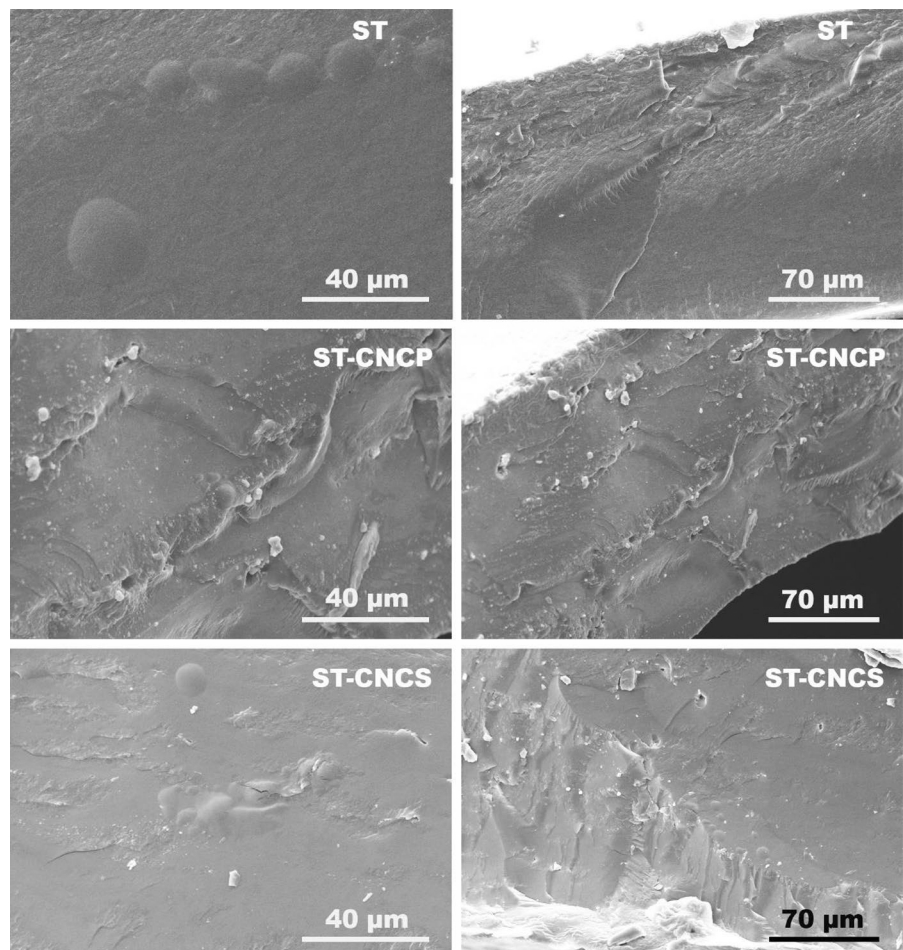
morphology of the bionanocomposite films surface became more structured with a rougher surface and no discernible cracks when 3 wt% of both CNCPs and CNCSs were added, indicating improved starch/CNCs interfacial adhesion (Kassab et al. 2019b). This enhanced compatibility between the two could possibly be attributed to the chemical similarity between starch and CNCs (Punia Bangar et al. 2022), as confirmed by FTIR analysis. Moreover, the CNCs are visible as white domains scattered throughout the films' fractured cross-section. Although the CNCs clusters within the ST were not apparent to the naked eye, the interaction between the CNCs and the polymeric phase may hardly be seen. On the other hand, due to the similarities of the CNCPs and CNCSs micrographs, it is difficult to determine which treatment (hydrolysis of phosphoric or sulfuric acids) gives the best CNCs dispersion and interaction with ST. Canigueral et al. (Cañigueral et al. 2009) claim that the accuracy of SEM is insufficient for accurately determining the dispersion of nanofiller in the film because only poor dispersions would be detectable using this method. One way to confirm the good

quality of filler dispersion and interaction with the matrix is the enhancement of mechanical properties (Agustin et al. 2013). The improvement in the mechanical performance is, in fact, largely attributed to the CNCs' superior dispersion and adherence to the polymer matrix (Punia Bangar et al. 2022).

Optical transparency of bionanocomposite films

The opacity of the elaborated bionanocomposites films plays a significant role in determining their quality. It also helps determine which of the two acid hydrolysis treatments (phosphoric acid and sulfuric acid) will produce a higher-quality film. Thus, the light transmittance of all the elaborated samples at 200–800 nm was studied using UV/Visible light spectroscopy and the results are presented in Fig. 10. UV radiation has wavelengths between 200 and 380 nm, whereas visible light ranges in wavelength from 380 to 780 nm. Despite having a shorter wavelength than visible light, UV radiation has a larger energy and accelerates oxidation more than visible light does (Tibolla et al. 2020). All bionanocomposites show

Fig. 10 **a** UV–visible spectra of ST-CNCP films, **b** UV–visible spectra of ST-CNCS films and **c** Schematic illustration of light transmission in ST-CNCP and ST-CNCS films
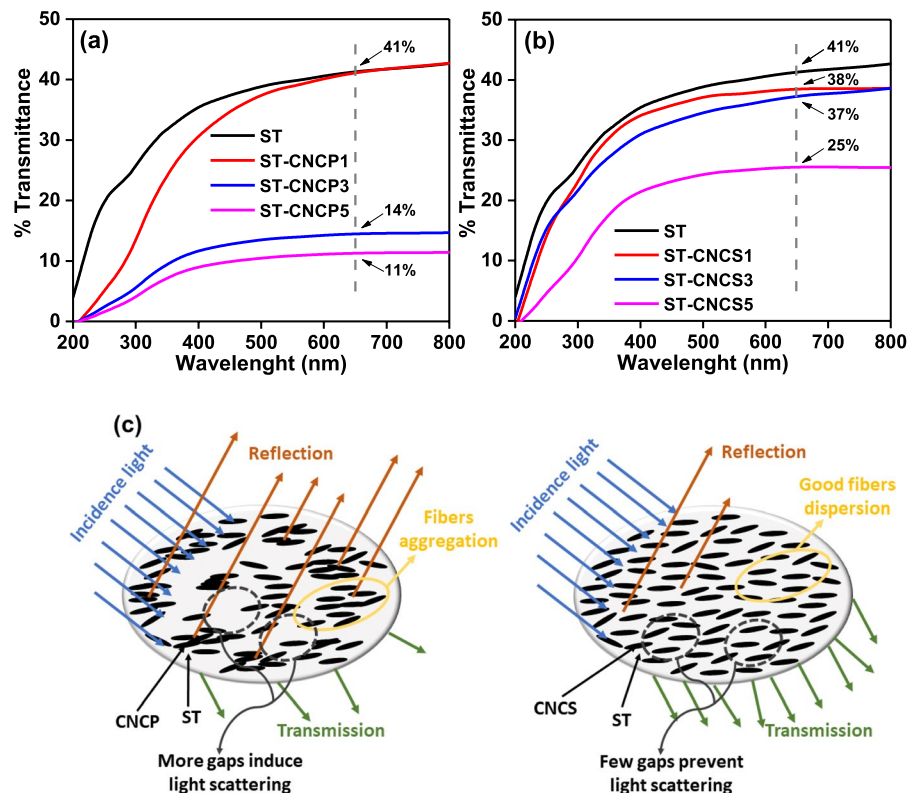
lesser light transmission than pure starch films across the whole spectrum of wavelengths examined. This occurs as a result of the fillers blocking the polymer matrix's ability to transmit light. Accordingly, the impact of nanosize can result in a uniform dispersion and a strong interaction between the nanofibers and the polymer matrix, resulting in a highly compact film with reduced light scattering effect (Tibolla et al. 2020; Yuan and Chen 2021). However, it can be clearly seen that CNCSs provides bionanocomposite films with better transparency than CNCPs ones (Fig. 10a, b). In fact, the light transmission at 650 nm decreases from 41% (ST film) to 11% and 25% for ST-CNCP5 and ST-CNCS5, respectively. The opacity and lower transparency of CNCP films compared to CNCS films can be explained by several factors. A common explanation is mainly related to the size of the filler. Indeed, the larger the particle size the lesser the light transmission due to the scattering of the visible light (Bodirlau et al. 2013; Kassab et al. 2020d), which is further confirmed by the AFM results where the particle size of CNCSs (31 ± 8.80 nm) is slightly smaller than that of CNCPs (43 ± 15.11 nm). Furthermore, a good dispersion of CNCs in the polymer matrix during the casting process has a significant impact on the transparency of the film. It has been reported that the residual sulfate group (SO_4^{2-}) provides a negative charge that improves the dispersion of CNCs compared to other types of acids (in this case phosphoric acid) (Septevani et al. 2022). Thus, the good dispersion of CNCSs in the starch polymer increases the transparency of the CNCS bionanocomposite films, since the gaps between the fibers are reduced and light scattering is prevented. In contrast, CNCPs promote fiber aggregation and the formation of voids in the film, which leads to greater light scattering and reduced light transmission (as illustrated in Fig. 10c) (Septevani et al. 2022). Finally, crystallinity was also reported to affect transparency. CrI of CNCSs was higher than CNCPs leading to the higher transparency of CNCS bionanocomposite films (Septevani et al. 2022).

To conclude, the elaborated bionanocomposite films are nevertheless regarded as transparent even if their opacity was higher than that of neat starch film. They exhibit less light transmission, which makes them suitable for use as packaging for oxidative products, for instance (Tibolla et al. 2020).

Thermal properties of bionanocomposite films

Thermogravimetric analysis is used to determine the impact of crosslinking hydroxyl and ester linkages in cellulose extracted using different acids (phosphoric acid and sulfuric acid) with that of hydroxyl groups in starch on the thermal stability of the elaborated bionanocomposite films. Hence, the thermal properties of the elaborated ST-CNCP and ST-CNCS films are shown in Fig. 11. The starch-based films' thermal degradation process exhibits three main steps of reaction (Fig. 11a, b), which are consistent with other studies (Bodirlau et al. 2013; Punia Bangar et al. 2022). The first weight loss between 65 and 100 °C represented the evolution of light volatiles together with an extra removal of bound moisture (Punia Bangar et al. 2022). The disintegration of the glycerol-rich phase of starch is responsible for the second thermal degradation, which took place between 100 and 200 °C (Punia Bangar et al. 2022). Finally, when heated beyond 200 °C (3rd weight loss), the thermal degradation rate accelerated due to the dramatic weight loss, which was caused by the partial disintegration of the starch-rich phase oxidation and the cellulose nanoparticles degradation (Bodirlau et al. 2013; Punia Bangar et al. 2022).

Regarding the effect of CNCs content on the maximum degradation temperature (DTG plots in Fig. 11a',b'), an insignificant shifting towards lower temperature values was observed in the elaborated bionanocomposite films with respect to the neat ST, meaning a good interaction between CNCs and ST matrix and/ or a moderate stability of the crystalline structure of CNCs (Montero et al. 2021). However, it is evident that the incorporation of CNCPs into ST polymer provides bionanocomposite films with better thermal stability than ST-CNCS ones. As was previously explained in the cellulosic fiber's characterization section, the capacity of phosphoric acid to produce char made them effective flame retardants. Thus, the high residual weight of ST-CNCP suggests that the ability of CNCPs to form char prevents ST from being exposed to heat sources (Gan and Chow 2019). Contrarily, the presence of sulfate groups in CNCSs, which breakdown at lower temperatures, is responsible for slightly reduced the thermal stability of the films (Kassab et al. 2020a). Finally, the obtained TGA/DTG results suggest that the as extracted

Fig. 11 Thermal properties of bionanocomposite films: **a**, **b** TGA and **a'**, **b'** DTG
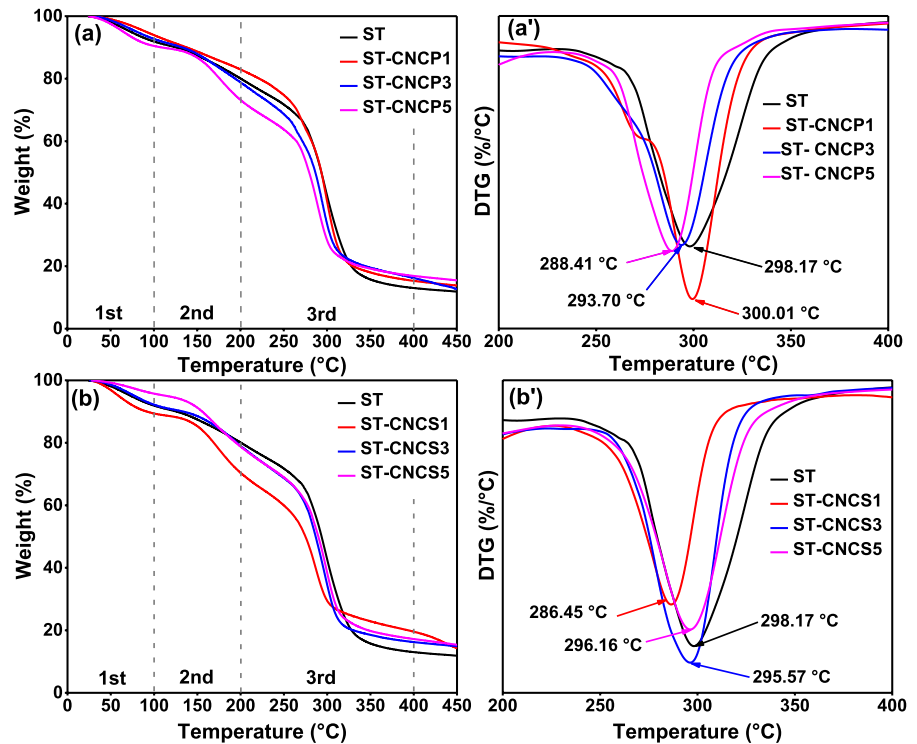
CNCPs and CNCSs can preserves relatively the bionanocomposite films' thermal stability.

Mechanical properties of bionanocomposite films

The reinforcing effects of CNCs in various polymeric materials have attracted a lot of attention over the past decade, and the findings have demonstrated that adding nanocrystals generally improved the mechanical properties of bionanocomposites (Li et al. 2014). The impact of utilizing two acid-derived CNCs (phosphoric acid and sulfuric acid) on the elaborated starch-based bionanocomposite films' tensile properties is of particular interest in this study. Hence, the typical stress–strain curves of the neat ST and its bionanocomposite films, as well as their representative young's modulus, tensile strength and strain at yield properties are presented in Fig. 12. The stress–strain curves often exhibit two characteristic regions of deformation behaviour (Fig. 12a). At low strains (the elastic region), the stress increases significantly with increasing strain and has a steep gradient, indicating that the chain is resistant to returnable extension in the elastic region (Cao et al. 2008; Tabassi et al. 2016). Higher strains (the plastic zone) were

accompanied by a gradual rise in stress without necking until the specimen broke. This behavior can be explained by the relatively homogeneous structure of the obtained bionanocomposite films (Cao et al. 2008; Tabassi et al. 2016).

It is common knowledge that the aspect ratio, fiber dispersion, and fiber-matrix compatibility of the reinforcement all play major roles in the mechanical performance of CNC-reinforced bionanocomposite films (Cañigueral et al. 2009). Thus, the observation of the final composite's tensile characteristics is one way to assess the success of these properties, as previously explained in the SEM section. Young's modulus, defined as the slope of the linear elastic deformation of the stress–strain curve, is a measure of the bionanocomposite ability to conserve mechanical energy during reversible elastic deformation; the higher the Young's modulus, the stiffer the material (Semlali Aouragh Hassani et al. 2022a). According to Fig. 12b, the elastic modulus of the elaborated films had a drastic increase with increasing CNCs loading level. Adding 5 wt% CNCs increase the films stiffness by 164% and 196% for ST-5CNCP and ST-5CNCS, respectively, with respect to neat ST. This increase can be associated with the introduction of

Fig. 12 Mechanical properties of bionanocomposites films. **a** Stress–strain curves, **b** Young's modulus, **c** Tensile strength, and **d** Strain at break
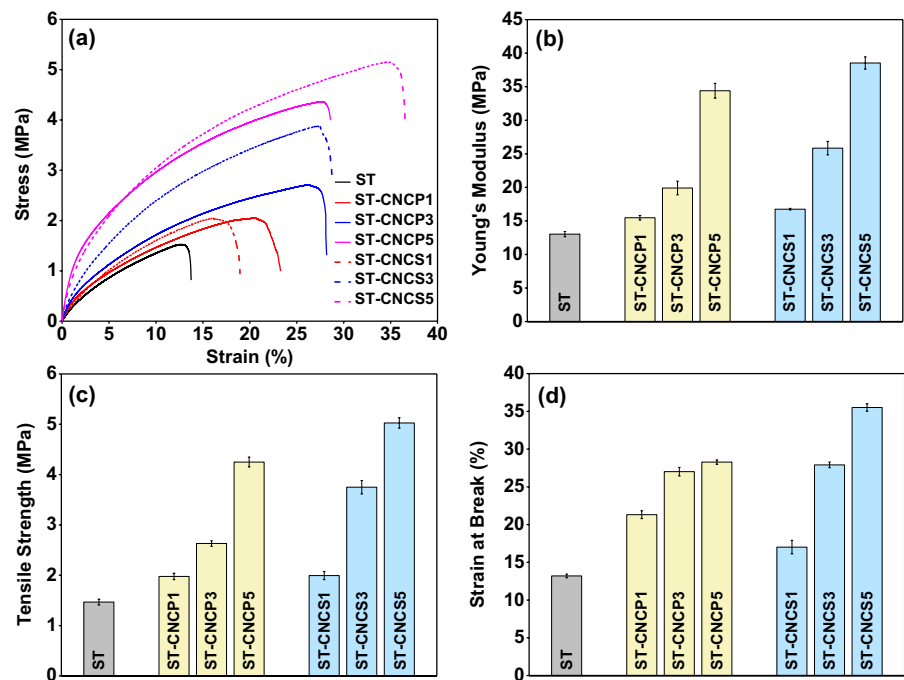
rigid CNCs nanoparticles (100–150 GPa) in the ST polymer (El Achaby et al. 2018a). In counterpart, the tensile strength represents the maximum stress value applied to the material, thus providing information about the fiber dispersion/distribution in the polymer, as well as their interfacial adhesion (Cañigueral et al. 2009). In our case, a linear dependence of the tensile strength with increasing CNCs content was clearly depicts (Fig. 12c). In fact, the addition of 5 wt% CNCPs and CNCSs significantly boosted the tensile strength of starch-based films by 190% and 245%, respectively. This is caused, in part, by the good dispersibility of CNCs in the ST matrix. Second, to the strong hydrogen bonding between the matrix and the reinforcement due to their similar chemical structure, thus resulting in effective stress transmission at the interface (Huq et al. 2012). This enhancement makes CNCs a more effective strengthening agent.

Finally, the strain at break indicates the flexibility and stretch of the film, and is determined at the breaking point under tensile testing (Tibolla et al. 2020). Generally, the incorporation of CNCs is known to improve considerably the young's modulus and tensile strength; while strongly reducing the film's strain at break even more than the neat polymer due to the limited mobility of the polymer chains (Reddy and

Rhim 2014). Surprisingly, raising CNCs content to 5% resulted in a 114% and 169% increase in elongation at break for ST-5CNCP and ST-5CNCS, respectively (Fig. 12d). This high degree of flexibility and ductility can be attributed to a synergistic boost from the flexible starch matrix, the helical layered structure of the CNCs and effective stress transfer via inherent strong CNCs/ST interaction, as previously described (Solouk et al. 2021).

Apart from that, it's evident that ST-CNCS bionanocomposite films exhibited much higher mechanical performances than ST-CNCP ones. Although the strain at break of the starch reinforced with 1 wt% CNCPs was found to be somewhat higher than that of 1 wt% CNCSs, this difference was minimal (less than 10%) and can be disregarded due to the error bars. Hence, the acid derived CNCs were found to have a tendency to alter the aspect ratio, morphological size, surface properties and degree of hydrogen bonding, significantly affecting the dispersion and mechanical behavior of the nanocomposites (Dhar et al. 2016). Based on the obtained results a clear correlation between the characteristic properties of CNCs and the optical transparency properties of ST-CNCs with the tensile properties of the bionanocomposite films can be found.

Indeed, as explained in the optical transparency section, the negative charge provided by the residual sulfate group (SO_4^{2-}), coupled with the presence of a high degree of intermolecular hydrogen bonding, leads to a significant improvement in the dispersion of CNCS in the ST matrix compared to the phosphoric acid-derived CNCs. This improved interaction is expected to effectively transfer the elastic modulus of CNCSs to ST and significantly improve the mechanical properties of the developed bionanocomposite films (Dhar et al. 2016; Septevani et al. 2022). On the other hand, the high aspect ratio, high surface areas and crystallinity of CNCSs compared to CNCPs also greatly contribute to higher reinforcement efficiency resulting in improved stress transfer from CNCSs to the ST matrix (Li et al. 2014). To conclude from these very important results, CNCs produced from newly discovered Raw pepper (Capsicum annuum L) stems residue provides a significant reinforcing impact on the tensile properties of the resulting bionanocomposite films.

Conclusion

In this study, phosphorylated (CNCPs) and sulfated (CNCSs) cellulose nanocrystals were successfully isolated from the newly identified pepper stems residue (Capsicum annuum L) as an unconventional cellulose-rich source. Firstly, cellulose microfibers (CMFs) with an average diameter of 16.40 ± 4.58 μm and crystallinity index of 80.12% were successfully produced using the conventional alkaline and beaching treatments. Subjecting the as-extracted CMFs to phosphoric and sulfuric acid hydrolysis treatment resulted in needle-like shaped nanocrystals (CNCPs and CNCSs) with a low diameter (43 ± 15.11 nm and 31 ± 8.80 nm), high crystallinity (84.78% and 85.41%) and relatively good maximum degradation temperature (341.90 °C and 341.50 °C°), respectively. Thereafter, the as-isolated CNCPs and CNCSs were separately dispersed in starch biopolymer (extracted manually from potatoes) at different weight loadings (1, 3 and 5 wt%), and their reinforcing effects on the chemical, morphological, thermal, transparency and mechanical properties of the resulted starch-based bionanocomposite films were investigated. According to the chemical structural study, the addition of CNCs to starch resulted in novel interactions indicating good interfacial adhesion. Remarkably, the SEM analysis scarcely shows any evidence of this interaction. In our instance, SEM's accuracy is insufficient to accurately evaluate the dispersion of nanofiller in the film, thus the improvement of transparency and mechanical characteristics of the developed films is the only approach to confirm the high quality of filler dispersion and interaction with the matrix. Globally, the incorporation of CNCs into starch biopolymer caused a substantial enhancement of these properties due to their rather similar polysaccharide structure and thus good interfacial interaction. However, the high aspect ratio, surface areas, and crystallinity of CNCSs, along with the negative charge provided by the residual sulfate group (SO_4^{2-}), resulting in a significant improvement in the dispersibility of CNCSs in the ST, leading to better transparency and mechanical properties compared to ST-CNCP films. This enhanced transparency can be seen in the decrease in light transmission (650 nm) from 41% (ST film) to 11% and 25%, respectively, for ST-CNCP5 and ST-CNCS5. While in term of mechanical properties, by adding 5 wt% CNCSs the films' rigidity, strength, and ductility are all increased by 164%, 190%, and 114%, respectively, as opposed to 196%, 245%, and 169% for ST-5CNCP, respectively, over neat ST. Conversely, the incorporation of CNCPs into ST polymer provides bionanocomposite films with better thermal stability than ST-CNCS ones. Apparently, the ability of phosphoric acid to generate char is effective as a flame retardant. The findings of this study are crucial for the right selection of cellulose nanocrystals as polymer composite reinforcements with outstanding moderated properties for diverse application.

Declarations

Conflict of interest The authors declare that they have no known competing financial interests. The manuscript has not been published elsewhere and that it has not been submitted simultaneously for publication elsewhere.

Consent for publication The authors give the publisher permission to publish the work.

Ethical approval The article does not include human participants and/or animals research.

Informed consent Informed consent was obtained from all participants.

References

Abd El-Mageed TA, Rady MM, Taha RS et al (2020) Effects of integrated use of residual sulfur-enhanced biochar with effective microorganisms on soil properties, plant growth and short-term productivity of Capsicum annuum under salt stress. Sci Hortic 261:108930. https://doi.org/10.1016/j.scienta.2019.108930

Ablouh EH, Kassab Z, Semlali Aouragh Hassani FZ et al (2022) Phosphorylated cellulose paper as highly efficient adsorbent for cadmium heavy metal ion removal in aqueous solutions. RSC Adv 12:1084–1094. https://doi.org/10.1039/d1ra08060a

Agustin MB, Ahmmad B, De Leon ERP et al (2013) Starch-based biocomposite films reinforced with cellulose nanocrystals from garlic stalks. Polym Compos 34:1325–1332. https://doi.org/10.1002/pc.22546

Anaya-Esparza LM, de la Mora ZV, Vázquez-Paulino O et al (2021) Bell peppers (Capsicum annum l.) losses and wastes: Source for food and pharmaceutical applications. Molecules 26:1–23. https://doi.org/10.3390/molecules26175341

Bahloul A, Kassab Z, El Bouchti M et al (2021) Micro- and nano-structures of cellulose from eggplant plant (Solanum melongena L) agricultural residue. Carbohydr Polym 253:117311. https://doi.org/10.1016/j.carbpol.2020.117311

Balakrishnan P, Gopi S, Sreekala MS, Thomas S (2018) UV resistant transparent bionanocomposite films based on potato starch/cellulose for sustainable packaging. Starch/staerke 70:1–34. https://doi.org/10.1002/star.201700139

Bodirlau R, Teaca CA, Spiridon I (2013) Influence of natural fillers on the properties of starch-based biocomposite films. Compos Part B Eng 44:575–583. https://doi.org/10.1016/j.compositesb.2012.02.039

El Bourakadi K, Semlali Aouragh Hassani FZ, El Achaby M, et al (2022) Packaging and bionanocomposites. In: Bionanocomposites for Food Packaging Applications

Cañigueral N, Vilaseca F, Méndez JA et al (2009) Behavior of biocomposite materials from flax strands and starch-based biopolymer. Chem Eng Sci 64:2651–2658. https://doi.org/10.1016/j.ces.2009.02.006

Cao X, Chen Y, Chang PR et al (2008) Starch-based nanocomposites reinforced with flax cellulose nanocrystals. Express Polym Lett 2:502–510. https://doi.org/10.3144/expresspolymlett.2008.60

Chen L, Kang YH (2014) In vitro inhibitory potential against key enzymes relevant for hyperglycemia and hypertension of red pepper (Capsicum Annuum L.) including pericarp, placenta, and stalk. J Food Biochem 38:300–306. https://doi.org/10.1111/jfbc.12048

de Azevedo LC, Rovani S, Santos JJ et al (2020) Biodegradable films derived from corn and potato starch and study of the effect of silicate extracted from sugarcane waste ash. ACS Appl Polym Mater 2:2160–2169. https://doi.org/10.1021/acsapm.0c00124

Dhar P, Bhasney SM, Kumar A, Katiyar V (2016) Acid functionalized cellulose nanocrystals and its effect on mechanical, thermal, crystallization and surfaces properties of poly (lactic acid) bionanocomposites films: a comprehensive study. Polymer 101:75–92. https://doi.org/10.1016/j.polymer.2016.08.028

El Achaby M, Kassab Z, Aboulkas A et al (2018a) Reuse of red algae waste for the production of cellulose nanocrystals and its application in polymer nanocomposites. Int J Biol Macromol 106:681–691. https://doi.org/10.1016/j.ijbiomac.2017.08.067

El Achaby M, Kassab Z, Barakat A, Aboulkas A (2018b) Alfa fibers as viable sustainable source for cellulose nanocrystals extraction: application for improving the tensile properties of biopolymer nanocomposite films. Ind Crops Prod 112:499–510. https://doi.org/10.1016/j.indcrop.2017.12.049

Espino E, Cakir M, Domenek S et al (2014) Isolation and characterization of cellulose nanocrystals from industrial by-products of Agave tequilana and barley. Ind Crops Prod 62:552–559. https://doi.org/10.1016/j.indcrop.2014.09.017

Espinosa SC, Kuhnt T, Foster EJ, Weder C (2013) Isolation of thermally stable cellulose nanocrystals by phosphoric acid hydrolysis. Biomacromol 8:187–203. https://doi.org/10.32604/jrm.2020.07940

Fareez IM, Ibrahim NA, Wan Yaacob WMH et al (2018) Characteristics of cellulose extracted from Josapine pineapple leaf fibre after alkali treatment followed by extensive bleaching. Cellulose 25:4407–4421. https://doi.org/10.1007/s10570-018-1878-0

Fortunati E, Luzi F, Puglia D et al (2015) Processing of PLA nanocomposites with cellulose nanocrystals extracted from Posidonia oceanica waste: innovative reuse of coastal plant. Ind Crops Prod 67:439–447. https://doi.org/10.1016/j.indcrop.2015.01.075

French AD (2014) Idealized powder diffraction patterns for cellulose polymorphs. Cellulose 21:885–896. https://doi.org/10.1007/s10570-013-0030-4

French AD, Santiago Cintrón M (2013) Cellulose polymorphy, crystallite size, and the Segal Crystallinity Index. Cellulose 20:583–588. https://doi.org/10.1007/s10570-012-9833-y

Gan I, Chow WS (2019) Synthesis of phosphoric acid-treated sugarcane bagasse cellulose nanocrystal and its thermal properties enhancement for poly(lactic acid)

nanocomposites. J Thermoplast Compos Mater 32:619–634. https://doi.org/10.1177/0892705718772866

Huang L, Xu H, Zhao H et al (2019) Properties of thermoplastic starch films reinforced with modified cellulose nanocrystals obtained from cassava residues. New J Chem 43:14883–14891. https://doi.org/10.1039/c9nj02623a

Huq T, Salmieri S, Khan A et al (2012) Nanocrystalline cellulose (NCC) reinforced alginate based biodegradable nanocomposite film. Carbohydr Polym 90:1757–1763. https://doi.org/10.1016/j.carbpol.2012.07.065

Jagadeesan S, Govindaraju I, Mazumder N (2020) An Insight into the ultrastructural and physiochemical characterization of potato starch: a review. Am J Potato Res 97:464–476. https://doi.org/10.1007/s12230-020-09798-w

Kassab Z, Aziz F, Hannache H et al (2019a) Improved mechanical properties of k-carrageenan-based nanocomposite films reinforced with cellulose nanocrystals. Int J Biol Macromol 123:1248–1256. https://doi.org/10.1016/j.ijbiomac.2018.12.030

Kassab Z, Boujemaoui A, Ben Youcef H et al (2019b) Production of cellulose nanofibrils from alfa fibers and its nanoreinforcement potential in polymer nanocomposites. Cellulose 26:9567–9581. https://doi.org/10.1007/s10570-019-02767-5

Kassab Z, Abdellaoui Y, Salim MH et al (2020a) Micro- and nano-celluloses derived from hemp stalks and their effect as polymer reinforcing materials. Carbohydr Polym 245:116506. https://doi.org/10.1016/j.carbpol.2020.116506

Kassab Z, Kassem I, Hannache H et al (2020b) Tomato plant residue as new renewable source for cellulose production: extraction of cellulose nanocrystals with different surface functionalities. Cellulose 27:4287–4303. https://doi.org/10.1007/s10570-020-03097-7

Kassab Z, Kassem I, Hannache H, Bouhfid R (2020c) Tomato plant residue as new renewable source for cellulose production : extraction of cellulose nanocrystals with different surface functionalities. Cellulose. https://doi.org/10.1007/s10570-020-03097-7

Kassab Z, Mansouri S, Tamraoui Y et al (2020d) Identifying Juncus plant as viable source for the production of micro- and nano-cellulose fibers: Application for PVA composite materials development. Ind Crops Prod 144:112035. https://doi.org/10.1016/j.indcrop.2019.112035

Kassab Z, Syafri E, Tamraoui Y et al (2020e) Characteristics of sulfated and carboxylated cellulose nanocrystals extracted from Juncus plant stems. Int J Biol Macromol 154:1419–1425. https://doi.org/10.1016/j.ijbiomac.2019.11.023

Khalili H, Bahloul A, Ablouh E et al (2023) Starch biocomposites based on cellulose microfibers and nanocrystals extracted from alfa fibers (Stipa tenacissima). Int J Biol Macromol 226:345–356. https://doi.org/10.1016/j.ijbiomac.2022.11.313

Li W, Guo R, Lan Y et al (2014) Preparation and properties of cellulose nanocrystals reinforced collagen composite films. J Biomed Mater Res Part A 102:1131–1139. https://doi.org/10.1002/jbm.a.34792

Liu S, Li X, Chen L et al (2018) Tunable d -limonene permeability in starch-based nanocomposite films reinforced by cellulose nanocrystals. J Agric Food Chem 66:979–987. https://doi.org/10.1021/acs.jafc.7b05457

Ludueña LN, Vecchio A, Stefani PM, Alvarez VA (2013) Extraction of cellulose nanowhiskers from natural fibers and agricultural byproducts. Fibers Polym 14:1118–1127. https://doi.org/10.1007/s12221-013-1118-z

Montero B, Rico M, Barral L et al (2021) Preparation and characterization of bionanocomposite films based on wheat starch and reinforced with cellulose nanocrystals. Cellulose 28:7781–7793. https://doi.org/10.1007/s10570-021-04017-z

Ouarhim W, Semlali Aouragh Hassani F, Qaiss A, Bouhfid R (2019) Rheology of polymer nanocomposites. In: Sabu Thomas, Sarathchandran, C. Nithin Chandran. Rheology of Polymer Blends and Nanocomposites Theory, Modelling and Applications. Elsevier, 1st Edition. pp 73–96

Oumayma M, Hassani FSA, El M et al (2021) Elaboration of a composite material based on plaster reinforced with phase change material/Oakum Fiber : physical, thermal and mechanical properties. J Energy Storage 35:1–10. https://doi.org/10.1016/j.est.2021.102321

Pozo C, Rodríguez-Llamazares S, Bouza R et al (2018) Study of the structural order of native starch granules using combined FTIR and XRD analysis. J Polym Res. https://doi.org/10.1007/s10965-018-1651-y

Punia Bangar S, Whiteside WS, Dunno KD et al (2022) Starch-based bio-nanocomposites films reinforced with cellulosic nanocrystals extracted from Kudzu (Pueraria montana) vine. Int J Biol Macromol 203:350–360. https://doi.org/10.1016/j.ijbiomac.2022.01.133

Rajinipriya M, Nagalakshmaiah M, Robert M, Elkoun S (2018) Importance of agricultural and industrial waste in the field of Nanocellulose and recent industrial developments of wood based Nanocellulose: a review. ACS Sustain Chem Eng 6:2807–2828. https://doi.org/10.1021/acssuschemeng.7b03437

Reddy JP, Rhim JW (2014) Characterization of bionanocomposite films prepared with agar and paper-mulberry pulp nanocellulose. Carbohydr Polym 110:480–488. https://doi.org/10.1016/j.carbpol.2014.04.056

Risite H, Salim MH, Oudinot BT et al (2022) Artemisia annua stems a new sustainable source for cellulosic materials: production and characterization of cellulose microfibers and nanocrystals. Waste and Biomass Valorization 13:2411–2423. https://doi.org/10.1007/s12649-021-01658-w

Salim MH, Kassab Z, Abdellaoui Y et al (2022a) Exploration of multifunctional properties of garlic skin derived cellulose nanocrystals and extracts incorporated chitosan biocomposite films for active packaging application. Int J Biol Macromol 210:639–653. https://doi.org/10.1016/j.ijbiomac.2022.04.220

Salim MH, Youness A, Ait Benhamou A et al (2022c) Influence of cellulose nanocrystals from pea pod waste on mechanical, thermal, biodegradability, and barrier properties of chitosan-based films. Cellulose. https://doi.org/10.1007/S10570-022-04587-6

Salim MH, Kassab Z, Ablouh E et al (2023) Cellulosic biocomposite foam papers impregnated by crosslinked starch /poly (vinyl alcohol) biopolymers. Ind Crop Prod 192:116074. https://doi.org/10.1016/j.indcrop.2022.116074

Salim MH, Kassab Z, Ablouh E-H, et al (2022b) Alfa fibers, their composites and applications. In: Plant Fibers, their Composites, and Applications. Woodhead Publishing, pp 51–74

Semlali Aouragh Hassani F, Ouarhim W, Raji M et al (2019a) N-silylated benzothiazolium dye as a coupling agent for polylactic acid/date palm Fiber bio-composites. J Polym Environ 27:2974–2987. https://doi.org/10.1007/s10924-019-01585-x

Semlali Aouragh Hassani F, Ouarhim W, Zari N et al (2019b) Injection molding of short coir fiber polypropylene biocomposites: prediction of the mold filling phase. Polym Compos 40:4042–4055

Semlali Aouragh Hassani F, El Achaby M, Bensalah MO et al (2020a) Injection molding of short fiber thermoplastic bio-composites: prediction of the fiber orientation. J Compos Mater 54:1–11

Semlali Aouragh Hassani F, Salim MH, Kassab Z et al (2022a) Crosslinked starch-coated cellulosic papers as alternative food-packaging materials. RSC Adv 12:8536–8546. https://doi.org/10.1039/d2ra00536k

Semlali Aouragh Hassani F, Chakchak H, El Achaby M, et al (2020b) Date palm fiber composites. In: Midani M, Saba N, Alothman OY (Eds) Date palm fiber composites: processing, properties and applications, 1st Edn. Springer, pp 75–91

Semlali Aouragh Hassani F, Ouarhim W, Kassab Z, et al (2021a) Mechanical characterization of cellulose nanoparticle-based advanced materials. In: Thakur VK, Frollini E, Scott J (Eds) Cellulose nanoparticles: volume 2: synthesis and manufacturing. pp 298–322

Semlali Aouragh Hassani FZ, Kassab Z, Achaby M El, et al (2021b) Mechanical modeling of hybrid nanocomposites based on cellulose nanocrystals/nanofibrils and nanoparticles. In: Cellulose Nanocrystal/Nanoparticles Hybrid Nanocomposites. pp 247–270

Semlali Aouragh Hassani FZ, El Achaby M, Qaiss A el kacem, Bouhfid R (2022b) Modeling of natural fiber-based biocomposites. In: Handbook of bioplastics and biocomposites engineering applications, 2nd Edn.

Septevani AA, Burhani D, Sampora Y et al (2022) A systematic study on the fabrication of transparent nanopaper based on controlled cellulose nanostructure from oil palm empty fruit bunch. J Polym Environ 30:3901–3913. https://doi.org/10.1007/s10924-022-02484-4

Simonovska J, Škerget M, Knez Ž et al (2016) Physicochemical characterization and bioactive compounds of stalk from hot fruits of capsicum annuum L. Maced J Chem Chem Eng 35:199–208

Solouk A, Xu K, Zhang Y et al (2021) Natural cuticle-inspired chitin / silk fibroin / cellulose nanocrystal biocomposite films : fabrication and characterization Natural cuticle-inspired chitin / silk fi broin / cellulose nanocrystal biocomposite films : fabrication and characterization

Sonia A, Priya Dasan K (2013) Chemical, morphology and thermal evaluation of cellulose microfibers obtained from Hibiscus sabdariffa. Carbohydr Polym 92:668–674. https://doi.org/10.1016/j.carbpol.2012.09.015

Tabassi N, Moghbeli MR, Ghasemi I (2016) Thermoplastic starch/cellulose nanocrystal green composites prepared in an internal mixer. Iran Polym J 25:45–57. https://doi.org/10.1007/s13726-015-0398-0

Tian C, Yi J, Wu Y et al (2016) Preparation of highly charged cellulose nanofibrils using high-pressure homogenization coupled with strong acid hydrolysis pretreatments. Carbohydr Polym 136:485–492. https://doi.org/10.1016/j.carbpol.2015.09.055

Tibolla H, Czaikoski A, Pelissari FM et al (2020) Starch-based nanocomposites with cellulose nanofibers obtained from chemical and mechanical treatments. Int J Biol Macromol 161:132–146. https://doi.org/10.1016/j.ijbiomac.2020.05.194

Warren FJ, Gidley MJ, Flanagan BM (2016) Infrared spectroscopy as a tool to characterise starch ordered structure—a joint FTIR–ATR, NMR, XRD and DSC study. Carbohydr Polym 139:35–42. https://doi.org/10.1016/J.CARBPOL.2015.11.066

Xie Q, Wang S, Chen X et al (2018) Thermal stability and crystallization behavior of cellulose nanocrystals and their poly(l-lactide) nanocomposites: effects of surface ionic group and poly(d-lactide) grafting. Cellulose 25:6847–6862. https://doi.org/10.1007/s10570-018-2086-7

Yadav M, Chiu FC (2019) Cellulose nanocrystals reinforced κ-carrageenan based UV resistant transparent bionanocomposite films for sustainable packaging applications. Carbohydr Polym 211:181–194. https://doi.org/10.1016/j.carbpol.2019.01.114

Yuan Y, Chen H (2021) Preparation and characterization of a biodegradable starch-based antibacterial film containing nanocellulose and polyhexamethylene biguanide. Food Packag Shelf Life 30:100718. https://doi.org/10.1016/j.fpsl.2021.100718